Automated measurement of fluorescence signals reveals a significant increase of the graft-derived neurite extension in neonates compared to aged rats

AUTHOR(S):

Grinand, Luc; Takahashi, Jun

CITATION:

Grinand, Luc ...[et al]. Automated measurement of fluorescence signals reveals a significant increase of the graft-derived neurite extension in neonates compared to aged rats. Regenerative Therapy 2022, 19: 97-106

ISSUE DATE:

2022-03

URL:

http://hdl.handle.net/2433/275964

Regenerative Therapy 19 (2022) 97–106

Contents lists available at ScienceDirect

Regenerative Therapy

journal homepage: http://www.elsevier.com/locate/reth

Original Article

Automated measurement of fluorescence signals reveals a significant increase of the graft-derived neurite extension in neonates compared to aged rats

Luc Grinand, Jun Takahashi*

Department of Clinical Application, Center for iPS Cell Research and Application, Kyoto University, Kyoto, Japan

ARTICLE INFO

Article history:
Received 13 December 2021
Accepted 12 January 2022

Keywords:
Neural graft
Parkinson's disease
Aging
Quantification
Automation

ABSTRACT

Background: — Neural tissue grafting is an acceptable form of cell therapy for brain injury and diseases. However, methods that can evaluate the graft integration and measure axonal extensions in a 3D environment are limited in scale, inconvenient, and operator intensive.
Method: — We stained grafts with a fluorescent antibody and then quantified the amount of fluorescence through the entire brain. To achieve this, we created an automated computer program designed to sort out authentic staining from background noise without any user input, enabling the analysis of thousands of images.
Results: — Our program could compensate for variations in the background brightness between images in all animals. Using this program, we show that human induced pluripotent stem cell (iPSC)-derived dopaminergic (DA) progenitor cells integrate better into the striatum of neonates than older rats.
Conclusion: — Our program can quantify quickly and conveniently the integration of neural grafts in a 3D environment without depending on a blinded human operator. We expect this method to be a useful tool to assess the efficiency of graft-enhancing treatments for neurodegenerative diseases or other neural reconstruction attempts.

1. Introduction

For the last thirty years, cell replacement therapies (CRT) have been gaining acceptance as treatments for neurodegenerative diseases, with Parkinson's disease as the primary model. Studies of fetal cell transplantation have shown the proof of concept [13]. The advent of embryonic stem cells (ESCs) and induced pluripotent stem cells (iPSCs) were milestones for CRT to be widely used clinically because of the limited availability of fetal tissue. Subsequent techniques aimed at obtaining the correct type of neurons from these cells and ensuring the absence of uncontrolled outgrowth of the graft have been developed. However, improvements in the therapeutic efficacy are still needed.

One of the factors determining the therapeutic effect is innervation by the grafted cells. But little is known currently about the molecular mechanisms that promote axonal extensions for CRT. Studies [2,3] found that grafted fetal mesencephalic tissue in the striatum of young rats showed more axonal extensions than in the striatum of older rats. However, accurate measurement of the axonal fibers remains difficult, especially in the 3D structure of the brain.

The two main metrics of axonal extension are fiber density and fiber area (Table 1). To measure fiber density, researchers will count the number of neurites manually in a region of interest [1,2,5,14], and to measure fiber area, they will measure how much area is covered by neurites in a series of micrographs [1,2]. Measuring the fiber density is preferred but has some concerns. First, counting individual neurites can only be performed when the number is relatively low. Second, this approach relies on sampling specific areas with high magnification, and a human operator does the counting, making this method heavily dependent on the operator's skill. Automatic counting is a solution, but without artificial intelligence or advanced pattern-recognition software, a computer

* Corresponding author. Department of Clinical Application, Center for iPS Cell Research and Application, Kyoto University, 53 Shogoin-Kawahara-cho, Sakyo-ku, Kyoto, 606-8507, Japan. Fax.: +81 75 366 7071.
E-mail address: jbtaka@cira.kyoto-u.ac.jp (J. Takahashi).
Peer review under responsibility of the Japanese Society for Regenerative Medicine.

https://doi.org/10.1016/j.reth.2022.01.002

cannot tell the difference between a line and a random arrangement of pixels. Thus, fiber area measurements are somewhat easier to perform, because the only challenge is to separate the noise and signal in the micrograph. To assess graft integration throughout the entire brain, in the present study, we sought a method to investigate axonal extensions as extensively as possible while minimizing user intervention.

We prepared an automation system that normalizes the background brightness for each image, calling this normalization the "base background". Next, incrementally more brightness is removed from every image in order to find the optimal brightness that distinguishes the signal from noise with minimal erosion of the signal. To test this system, we transplanted human iPSC-derived dopaminergic (DA) progenitor cells into the rat striatum of different age groups and stained the brains against hNCAM, enabling clear visualization of the extended axonal fibers. Using our approach, we confirmed that younger brains are more supportive for axonal extensions than older brains and could quantify the magnitude of the difference.

2. Material and methods

2.1. iPS culture and DA progenitor differentiation

Grafted DA progenitors were induced from an iPSC line (1231A3) established from the peripheral blood cells of a healthy individual [9]. Culturing, differentiation and sorting were performed following a protocol described previously [4].

iPSCs were cultured in StemFit AK02 medium (Ajinomoto) at 37 °C on laminin 511-E8 fragment (iMatrix 511Silk, Matrixome)-coated plates. The medium was changed every one or two days depending on the cell density. Passages were performed once a week, and new maintenance plates were prepared at a density of 1560 cells/cm^2 (9×10^4 cells for a 6-well plate) in the same medium supplemented with 10 μM Y-27632 reagent (Wako) to prevent cell death. The cells were detached by adding 0.5X TrypLE Select (ThermoFisher) for 5 min at 37 °C and centrifuged to remove the enzyme before replating.

DA differentiation was initiated by replating the iPSCs at a density of 5.2×10^5 cells/cm^2 ($=5 \times 10^6$ cells per well of a 6-well plate) in GMEM (Gibco) and 8% KSR (Gibco) with laminin 511-E8 fragment coating. The medium was supplemented with 10 μM Y-27632 reagent on the first day of differentiation (day 0), 0.5 μM A-83-01 (Wako) on days 0–6, 2 μM Purmorphamine (Wako) and 0.1 μg/mL FGF8 (Wako) on days 1–6, 3 μM CHIR99021 (Wako) on days 3–11, and 0.1 μM LDN193189 (Stemgent) on days 0–11.

On day 12, the cells were detached using 1X TrypLE Select for 10 min and pooled in 4 °C sorting buffer (Phosphate Buffered Saline (Nacalai tesque), 20 mM glucose (Wako), 2% fetal bovine serum (BD), 80 mg/L Gentacin (TaKaRa) and 10 μM Y-27632. The cells were then stained with 100 ng/mL custom-made phycoerythrin anti-Corin antibodies (a gift from the KAN Research Institute) for 20 min, washed twice with sorting buffer, and sorted using an Aria III FACS machine (BD Biosciences).

The sorted cells were re-analyzed to ensure at least 95% purity and plated to form spheres in U-bottom non-adhesive 96-well plates at a density of 2×10^6 cells/plate (2×10^4 cells/well) in Neurobasal medium (Gibco) supplemented with B27 (2%, Gibco), 0.2 mM Ascorbic Acid (Towa), 0.5 ng/mL BDNF (Wako), 10 ng/mL GDNF (Wako) and 0.4 mM dbcAMP (Daiichi Sankyo). To the medium immediately post-sorting was added 10 μM Y-27632 reagent and 1% Penicillin/Streptomycin (Gibco). The medium was changed every three days by replacing half of it (starting from 150 μL/well) and replenished when necessary to account for evaporation.

At day 28 of the differentiation, the spheres were pooled in a large dish (Ø8-10 cm) placed on a dark background. The spheres were then manually picked with a pipette in packs of 20, each of which was stored in a 0.5 mL tube half full of supplemented Neurobasal medium plus 1% Penicillin/Streptomycin and kept on ice. Spheres in each tube were re-counted under a microscope to ensure the proper number was present immediately prior to the transplantation.

2.2. Animals

Animals were cared for and handled according to the Regulations on Animal Experimentation at Kyoto University under approval by the CiRA Animal Experimentation Committee. F344/NSlc SD Norway rats (Shimizu, Japan) were used in the experiments and hosted in plastic boxes by groups of two or three in the specific pathogen free area at the Center for iPS Cell Research and Application, Kyoto University. Males and female were kept separate on a day/light cycle of 12 h and had *ad libidum* access to food and water. The temperature was set at 23 ± 2 °C, and the humidity at 50 ± 5%. Litter was changed every two or three days. Six two-year-old rats (3 females, 3 males) and 7 neonates from the same litter (3 females, 4 males) were used in the experiments. Two older male rats died before the end of the two-month period between grafting and sacrifice, and two male neonates were excluded from the analysis because their grafts were misplaced, leaving images from 5 neonates and 4 older rats for the analysis.

2.3. Grafting

The animals were first anesthetized with a 50/50 mix of O_2 and N_2O supplemented with 2% Isoflurane (Wako) and then attached to a stereotaxic injector (Narishige). In the case of neonates (5-days old), because the ear bar could not be used, the animals were taped into position on a heating plate set to 37 °C. In addition, all distances for targeting the striatum were halved, since the size of the neonate brain is approximately half that of the adult brain.

The front skin of the animal was then cut to expose the skull, and a hole was drilled 3 mm to the right and 1 mm anterior of the Bregma. The skull was drilled until the bone was so thin it could easily be pierced by the tip of sharp tweezers and without burning

Table 1
Summary of graft integration measurement methods. All studies listed used Parkinson's disease rodent models. "Fiber density" counts fibers in a set area. "Fiber area" measures how much of an image is covered by neurites.

Article	Graft	Metrics	Comparison
[3]	Fetal extract ± Schwann C.	Fiber area / maximum Fiber density	Various ages, lesion duration, and co-grafts
[5]	Fetal & ESC derived	Fiber density	Fetal vs ESC graft
[2]	Fetal extract	Fiber density / Fiber area	Young adult vs Adult vs Old rats
[11]	Fetal extract	Fiber density	With / without GDNF releasing capsule
[1]	Patterned ESC	Fiber density / Fiber area	Time after transplant
[14]	Fetal extract	Total neurite length / Fiber density	With / without rehabilitation

the bone through friction. A pre-hole was formed by lowering a sharp-tipped syringe (Hamilton 80,330) 5.5 mm into the brain (0 being the surface of the brain, not the skull).

Twenty DA neurospheres (each being composed of 20.000 cells) were placed on the inner side of a piece of parafilm. The cell culture medium was carefully pipetted away in order to leave only the spheres and a minimal amount of solution. The spheres were then loaded into a blunt-end, zero dead volume Hamilton syringe (Hamilton 88,000) that had been previously hydrated with cell media. The total volume loaded into the syringe was preferably kept under 1 μL.

The loaded syringe was then set into the stereotaxic injector and lowered slowly 5 mm into the brain. The cell mix was injected at a speed of 0.5 μL/min. The syringe was left in place for 3–5 min in order to let the pressure dissipate and was then removed slowly.

2.4. Cyclosporine A treatment

In order to avoid graft rejection, 10 mg/kg cyclosporine A (LC Laboratories, C-6000) was injected into the animal either immediately before or after the transplantation as well as every day for the next 4 days (5 days total). The injection was peritoneal for old rats and subcutaneous for neonates (under the skin between the shoulder blades) to avoid piercing the intestines.

The cyclosporine solution was prepared from 1 g of cyclosporine powder dissolved in 6 mL pure ethanol (Wako) and then supplemented with 4 mL Kolliphor (also known as Cremphor; Sigma). After intense vortexing, the solution was split into ten 1 mL aliquots that were kept in the dark at 4 °C. Each aliquot was diluted with 9 mL saline before use to obtain the working solution of 10 μg/mL. The working solution was further diluted in saline in order to obtain a volume practical for handling and injecting under the skin of a 10 g neonate (around 5 μL).

2.5. Euthanasia & sample preparation

Two months after the transplantation, all animals were sacrificed by injecting a lethal dose of pentobarbital (Schering Plough). The thorax of the animal was then opened, and a syringe was inserted into the left ventricle while the right atrium was cut open. Blood was flushed out of the animal's circulatory system by pumping PBS in the ventricle through the syringe and eventually flowed out of the cut atrium. Once the blood was sufficiently washed out, PBS was replaced with 4% paraformaldehyde (PFA, Muto Pure Chemicals) and pumped in the animal's circulatory system until fixation was deemed sufficient. Brains were recovered, and each was placed into 50 mL of 4% PFA for at least 24 h. Next, they were placed into 30% sucrose (Nakalai tesque) for one week for cryoprotection. Afterwards, the brains were frozen in a block of OCT compound (Sakura) and stored at −30 °C in an airtight bag until cryosectioning. Brains were cut into 40-μm thick coronal sections, starting slightly before the most anterior point of the corpus callosum and extending until the appearance of the cerebellum. Sections were kept in anatomical order at −30 °C in 24-well plates and stored in antifreeze solution (40% PBS, 30% Ethylene Glycol (Wako), 30% Glycerol (Nakalai tesque)).

2.6. Immunostaining

Staining was performed on every fourth slice. Antifreeze was washed away with excess PBS. Then, floating slices were washed with PBS and 0.1% Triton X-100 (PBST) three times for 5 min each, blocked for 1 h in PBST + 0.5% normal donkey serum (NDS, Millipore), stained with primary antibody overnight at 4 °C in PBST + 0.5% NDS, washed in PBST again three times for 5 min each, stained with secondary antibody in PBST + 0.5% NDS for 2 h at room temperature in the dark, and finally once more washed with PBS three times for 5 min each. The sections were then mounted on MAS-01 coated glass slides (Matsunami Glass) with Dako mounting medium (Dako S3023).

The antibodies used were Santa Cruz anti-hNCAM “Eric1” (SC-106, 200 μg/mL diluted at 1/200) and Donkey Alexa Fluor 488-conjugated anti-Mouse IgG Antibody (Invitrogen A-21202, 2 mg/mL diluted at 1/500).

2.7. Imaging

Images of the seriated sections were taken using a Yokogawa CQ1 confocal microscope with the following settings: magnification 10×, lamp power 50%, exposure time 500 ms, 5 Z-levels covering 20 μm, and soft focus enabled. Z-sections were later compacted into one image, keeping the maximum intensity for each pixel.

In all rats, all areas where hNCAM staining was observed or expected was imaged.

2.8. Macro operations

See Supplementary materials for the macro code and user interface.

2.8.1. Automated normalization of the “base” background

Because large parts of the brain were imaged, the collection of images contained different types of tissues with different amounts of autofluorescence and non-specific antibody binding (Fig. 1). We designed an automated system that normalized each image (this normalization is called the “base background” hereafter).

Our system determined the base background of each image by sampling several small areas in the image. For each area, the mean (Mean) and standard deviation (SD) were measured, and the two were used to discriminate different regions of the brain as follows:

- Ventricular space: low Mean, very low SD
- Neurite-free brain tissue: moderate Mean, moderate SD
- Neurite-containing tissue: moderate to high Mean, high and variable SD
- Mixed contents: variable Mean, high SD

The SD/Mean ratio was used to discriminate the four types of regions. The precise ranges of the ratio for the discrimination are decided by the user. In particular, a ratio that identifies the neurite-free brain tissue is needed. In the present report, we used a SD/Mean ratio of 10% ± 2%.

Sampling of the small areas was not done at random but at predetermined locations that are common to every image. We sampled 30 regularly-spaced areas (Fig. 2). For each small area, the SD/Mean ratio was calculated. If the ratio indicated neurite-free host tissue, the mean brightness was used to calculate the base background for the image. Should multiple small areas be identified as neurite-free, the average of the means was used to calculate the base background. The base background was then subtracted from the signal intensity of all pixels in the image.

The SD/Mean ratio of 10% ± 2% was selected because it appeared relatively constant during observation of the images by the operator. Different neighboring ratios have been tested (from 8 to 12%) with different tolerances (±1 to ±3%) but those mostly resulted in more images failing the autodetection, lowering the quality of the analysis (data not shown). For detailed guidance regarding how to

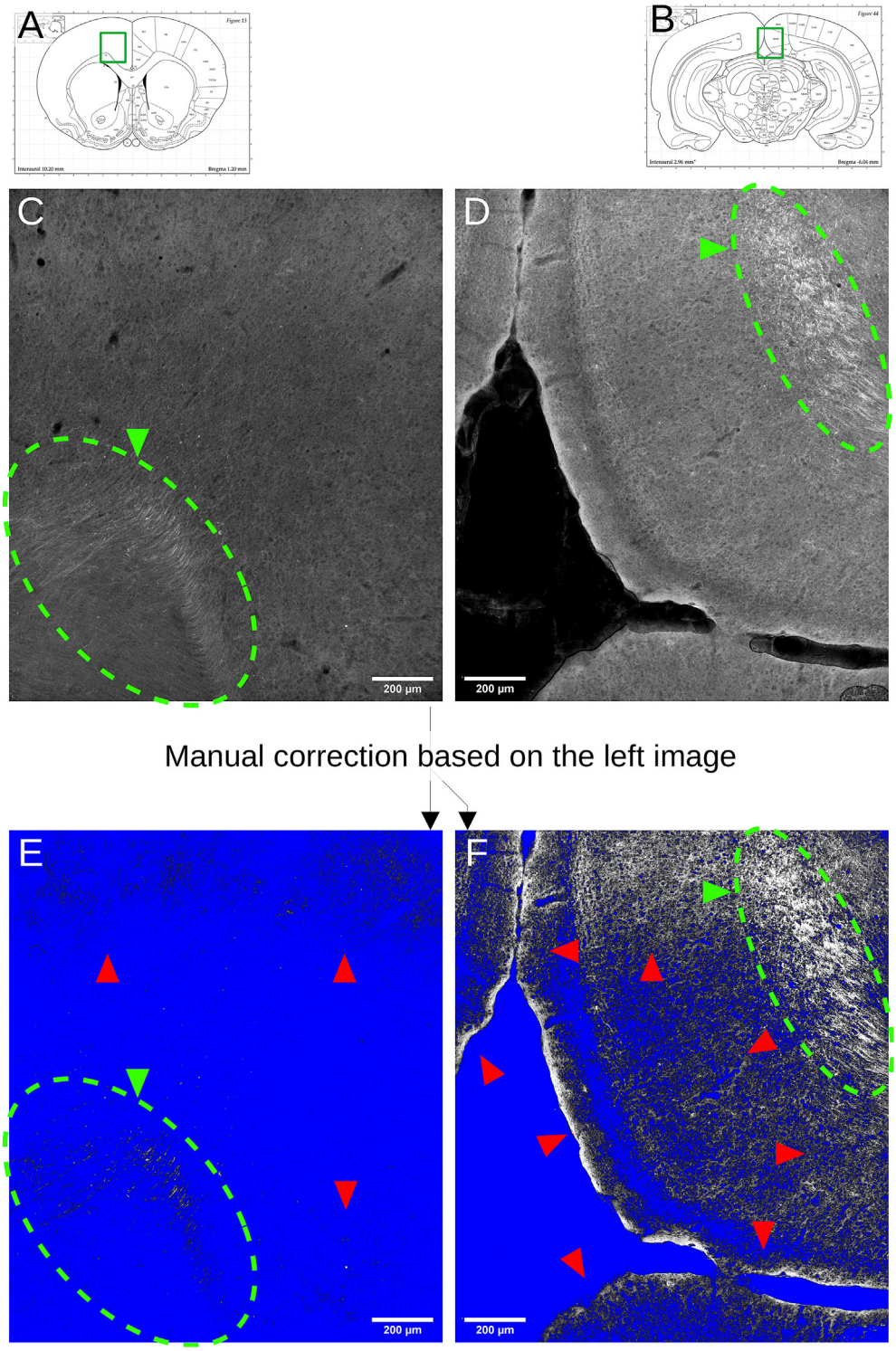

Fig. 1. The amount of background noise to filter in one image may not be appropriate for a different image. A&B: Approximate location of the images displayed below (C&D). The images come from the same animal and were stained at the same time. C&D: Original images adjusted to the same visualization settings. Areas outlined in green represent graft-derived fibers. E&F: Hi-low visualization after filtering (blue = zero, otherwise greyscale). E: Image C after subtracting 400 PBU (Pixel Brightness Units), this correction isolates the neurites (inside the green dotted line) while minimizing the noise (red arrowheads). F: Image D after removing 400 PBU still shows large amounts of unspecific signal. Conversely, treating image C with a filtration appropriate for image D erases almost the entire content of the image (not shown).

determine the appropriate ratio for a third party, please refer to the "User manual" (supplementary data).

Should the test fail on all the 30 areas (i.e., none identified as neurite-free), the program generates a failure report for manual verification and uses the base background determined for the previous image, provided this image is from the same brain slice. Otherwise, the image is rejected from the analysis. This strategy can lead to images being rejected in cascade.

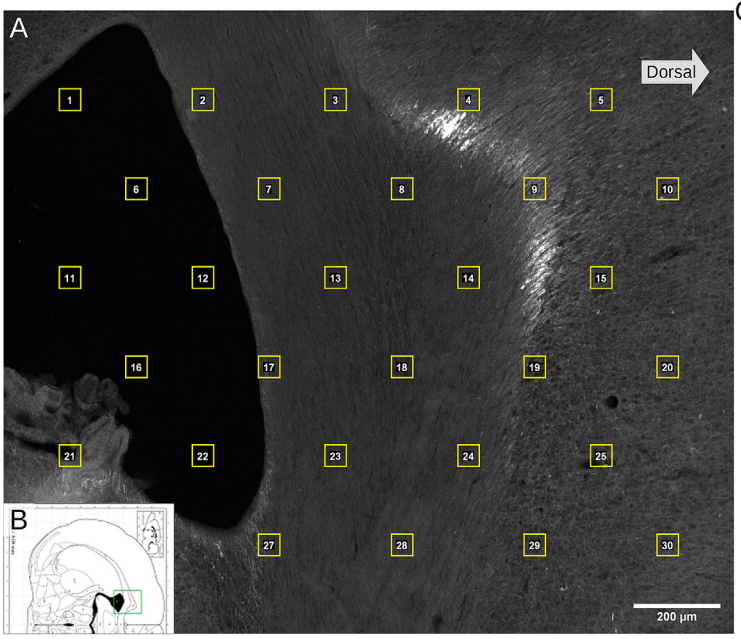

C

Label	Mean	SD	SD/Mean	test
1	118.572	6.420	0.054	fail
2	352.676	26.000	0.074	fail
3	332.647	27.227	0.082	pass
4	417.639	46.422	0.111	pass
5	370.313	46.650	0.126	fail
6	115.450	4.925	0.043	fail
7	310.529	22.045	0.071	fail
8	302.373	27.164	0.090	pass
9	472.080	80.560	0.171	fail
10	381.112	61.714	0.162	fail
11	108.851	4.006	0.037	fail
12	115.082	4.975	0.043	fail
13	300.816	22.629	0.075	fail
14	316.379	26.999	0.085	pass
15	367.037	49.598	0.135	fail
16	115.330	5.392	0.047	fail
17	337.489	30.898	0.092	pass
18	291.468	28.047	0.096	pass
19	336.051	71.017	0.211	fail
20	368.737	40.700	0.110	pass
21	298.923	137.029	0.458	fail
22	118.475	5.717	0.048	fail
23	310.236	25.530	0.082	pass
24	335.132	34.714	0.104	pass
25	336.567	89.341	0.265	fail
26	424.612	61.276	0.144	fail
27	352.856	49.633	0.141	fail
28	358.209	24.319	0.068	fail
29	357.329	46.307	0.130	fail
30	397.583	43.704	0.110	pass

Fig. 2. An automated decision process determines the base background. A: Sample image on which 30 sampling areas are overlaid (locations are fixed for all images). B: The schematic indicates the approximate location of the image (Box 26 is under this schematic.). C: Table of local areas and the properties of their contents. Each area is tested for $0.08 < \frac{SD}{Mean} < 0.12$. The mean brightness of areas that passed the test were averaged to give the base background (340 PBU for this image).

2.8.2. Optimized background filtering

Subtracting the base background solves the variability issue between images but is not sufficient for filtering background noise. Thus, after subtracting the base background from the images, another fixed number of pixel brightness units (PBU) are removed, and the number of positive pixels, which indicates graft-derived neurites, is counted. This number of PBU subtracted is iterated until a number set by the user (Fig. 3; see User Manual in Supplementary Materials). The total deleted PBU in an iteration is referred to as the "filtration level". The user can then make a graph with the resulting data to choose the best filtration level (Fig. 3E). In practice, the program applies one filtration level for all images in the dataset before iterating and stores the data per slice instead of per filtration level. This allows the user to plot the results on the antero–posterior axis and makes the program easier to restart in case of interruptions.

Another way to understand this process is to consider that the amount of remaining background noise is unknown, and by eroding the brightness of all pixels little by little, we should reach a point where all noise is gone, allowing us to compare an equally degraded but "pure" signal.

2.9. Statistical analysis

After the last iteration in 2.8.2, the raw per-slice data is compacted by the macro to obtain the total number of positive pixels per animal and per filtration level. Bilateral unpaired student t-tests were performed for each filtration level using LibreOffice Calc by calling the csv files generated by the macro, and the resulting p-values were used to obtain an indicator $\left(indicator = \frac{100}{p-value}\right)$ for visualization purposes (hence, for p-values <0.05, the indicator is > 2000).

Additionally, the improvement factor of the Neonate group relative to the old group $\left(\frac{Neonate\ average\ pixels - Old\ average\ pixels}{Old\ average\ pixel}\right)$ was calculated. Testing the normality of the distribution of base backgrounds was done by generating random numbers based on a theoretical normal distribution of identical mean and SD. The values from both the base background set and randomly generated set were sorted in ascending order, and the "correlation coefficient" function in LibreOffice Calc gave the result.

2.10. Quality control

In order to verify the results of our automated base background measurement process, we prepared a subset constituted of 6 images per animal (each animal having approximately 300 images taken throughout its brain). They were selected randomly but with enough spacing between them to represent various parts of each animal's brain.

On each of those images, the operator selected three hand-drawn signal-free areas (each being 1–2% of the image size) in which the mean brightness was measured, the average of those three values becoming the "manual value". Next, the program obtained the "autodetection" value by checking the contents of the 30 squares on each image as described in section 2.8.1. Finally, both values were matched for each image, and the correlation coefficient was obtained using the LibreOffice Calc function of the same name.

To investigate the rate of false positives (squares passing the "test" as explained in section 2.8.1 while being inappropriate), we ran a purpose-build macro that only recorded which square passed or failed on each image of the previous subset. The resulting data was then reviewed manually, and squares that were deemed problematic were counted.

3. Results

First, we performed quality control on a subset of 54 randomly selected images, comparing the results of the automated base background determination step with the values a human operator obtained by manually measuring background noise intensity (Fig. 4). Both methods returned slightly different values, as expected, but showed a strong correlation with R reaching 87.6%. It

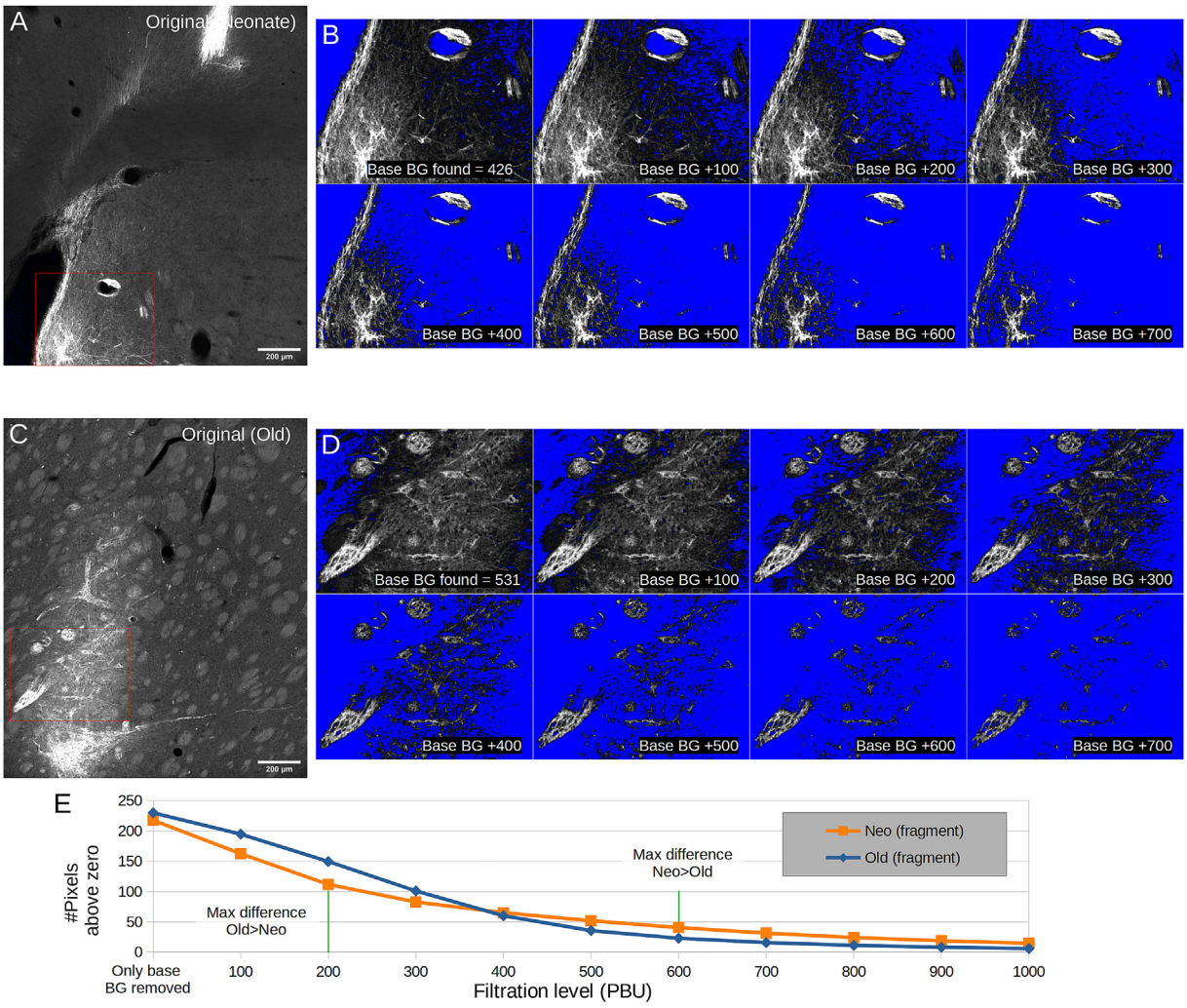

Fig. 3. Automated search for the optimal brightness correction. A&C: Original images before any correction. The red rectangles are magnified in the B&D series of images. B&D: Application of different filtration levels after base background (BG) was applied. Numbers indicate filtration levels in PBU. E: Total positive area (non-blue) in the magnified regions. With only two samples in this case, no statistical analysis was performed, thus it is not possible to tell which filtration level is optimal based on p-value, but extrema are highlighted. The optimal filtration level for the entire dataset can be found by extending this approach to every image of every animal. Clear improvement can be seen for filtration levels +200 to +400, as large areas containing a dim signal (black) are erased and start to appear blue. On the other hand, filtration levels of +600 or +700 show only minor changes.

indicates that our automated base background detection constitutes a consistent approximation of what an operator would do.

Separating these points according to the group they belong to ("Old" versus "Neonate") and running a T-test showed that there was no significant difference in the background values measured, either manually or automatically, indicating that aging does not fundamentally alter the background fluorescence of brain tissue. Additionally, reviewing individual "passing" squares on the same subset of images showed that out of the 786 passing squares (which amounts to 14 passing and 16 failing on average in the process described in Fig. 2), only eight were deemed problematic by the operator, giving a false positive rate of 1%. All of those were considered inappropriate due to containing non-negligible amounts of genuine hNCAM staining.

Running the analysis on our entire dataset (9 animals, 3145 images total) took approximately 11 h on an average 2017 Dell desktop computer. Again, the automatically determined base backgrounds showed no alarming differences between the neonate and old groups, nor among individuals. This also suggests that the sample preparation and imaging were consistent across animals (Fig. 5). A total of 26 images failed the base background test, such that 12 inherited the base background of the previous image and 14 were rejected entirely (10 in the neonate group and 4 in the old group). Most images (69%) were attributed a base background value

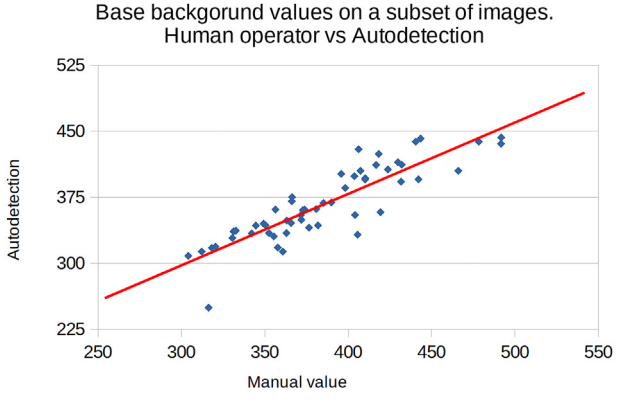

Fig. 4. Correlation between the result of the autodetection and manual measurement by the operator. Each blue dot represents one image, the red line is the linear regression. The correlation coefficient between the abscissa and ordinate is R = 87.6%.

between 350 and 425 PBU. Overall, the distribution of the base backgrounds resembled a normal distribution (94% correlation with a normal distribution of identical Mean and SD). However, a few images displayed very high base backgrounds (above 500 PBU, Fig. 5A) that rarely appear in a normal distribution of identical properties.

Filtration levels (section 2.8.2) ranged from 100 to 1800 PBU in increments of 50 PBU. In order to assess the efficacy of the base background, we ran the filtration levels with and without the base background (Fig. 6). We also calculated the p-value between Neonate and Old rats at each filtration level, and plotted 100/p as an indicator for the probability of the difference. At very high filtration levels, we can see a steady decay of the 100/p indicator, meaning differences become smaller and smaller due to excessive filtering.

In graphs A and B of Fig. 5, the indicator shows statistical significance for filtration levels between 400 and 700 PBU, with a maximum (i.e., minimal p-value) at 500 PBU when the base background is applied. Compared to the condition without the base background, all traces appear to have shifted leftward and converged because a variable amount of luminosity (i.e., the base background) was removed from each image (on average, 375 PBU; see Fig. 5B). Particularly, we can see that applying the base background corrects the trace of rat Old A (Fig. 6, graphs A and D), which appeared offset from the other older rats in a way reminiscent of the differences in average base backgrounds between old rats in Fig. 5B. Similarly, the signal for Neo E shows a different pattern from the other neonates (Fig. 6, graphs A and D). By searching the recorded data relative to base backgrounds (see Supplementary materials section 3.3), we identified 6 images that had very high base backgrounds which may be the cause of this anomaly in the curve shape. Consequently, the variation among animal groups is reduced (Fig. 6, graphs B and E), which in turn leads statistical significance to be more manifest, both through how many filtration levels return $p < 0.05$ and how small the minimal p-value obtainable is (Fig. 6, green lines).

Among the filtration levels that return statistical significance (light green areas, Fig. 6, graphs C and F), the amount of signal measured in the Neonate group ranges from 32.2% greater than in the old group, to 42.6% greater than the old group with the base background. Without the base background, similar improvement rates are obtained, ranging from 35.8% to 39.7% more signal in the neonate group. Among those, the difference in measured signal that shows the minimal p-value (0.0338) would be for "base background +500 PBU", with Neonates displaying 38.9% more signal. The maximum believable difference between both groups (i.e., disregarding filtration levels 100 to 600 of graph F, Fig. 6) is however not within the range of base backgrounds where differences are significant.

Interestingly, we also observed that our indicator (=100/p) started to rise when a filtration level of 300–400 PBU was applied in addition to the base background and when a filtration level of 700–800 PBU was applied without the base background (Fig. 6, graphs B and E). This observation agrees with the apparent brightness of the numerous specks we observed scattered across older brains (around 600–700 PBU, Fig. 7), which we presumed to be cellular debris. These specks pose a non-negligible hindrance to an operator trying to separate a fluorescent signal from the background manually.

4. Discussion

In general, measuring the extension of graft-derived neurites in a host brain has required an operator to count the neurites (Table 1). The heavy dependence on the operator makes the analysis inaccurate, tedious and limits the scale of observation. In response, we designed a macro that gives each image a customized noise correction (base background) and searches for parameters that best reveal differences between groups (filtration levels) irrespective of the amount of data.

Our system quantifies the area on an image that contains appreciable fluorescence, which is intended to represent both the fiber length and fiber count, without having to dissociate these two factors. This strategy has been used by several groups [1,2,14]. Our automated findings agree with [1]; who applied a Gaussian blur to their images before thresholding, and [2]; who used a thresholding step based on neurite-free areas to extract their data. Both of those methods output a measure of the same type as ours.

Another approach to measure engraftment is to count the number of neurites crossing arbitrary lines placed at a set distance from the graft [11,14]. A variation of this principle is the "space ball probe" [2,5], which relies on taking multiple high magnification optical sections of a location and placing a virtual sphere inside the 3d stack. The number of neurites intersecting the sphere is fed to an equation that outputs fiber density. The arbitrary line method relies on the operator placing the lines at the desired locations. Those lines can only be placed in the brain sections that remain close to or contains the graft core, thus strongly limiting the scale of observations. As for the space ball probe method, an overview of the fiber density throughout the entire brain with this method would require manually selecting and imaging countless areas at high magnification.

On the other hand, our system is not restrained to any area of the brain and can extract data from images despite low magnification and moderate quality. While it is true that extracting data from

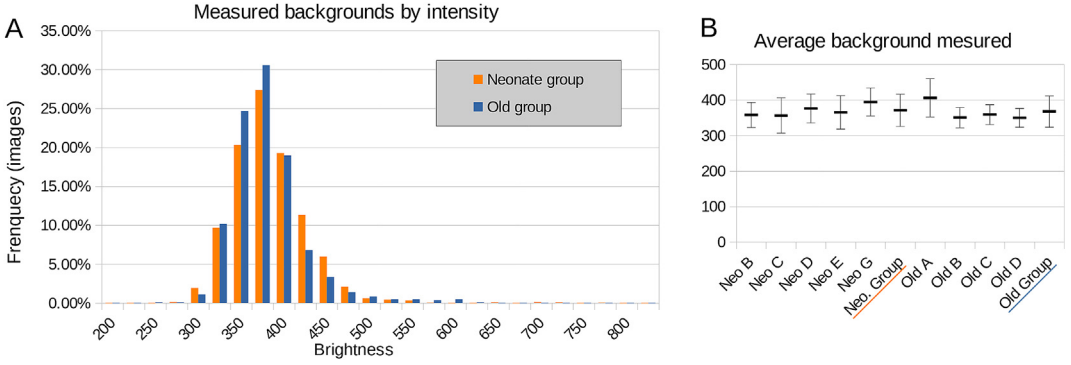

Fig. 5. Base backgrounds of all 3145 micrographs of our dataset as measured by the technique described in Fig. 2. A: Histogram of base backgrounds (Mean = 370, SD = 44.5). The measured values show a 94% correlation with a random normal distribution of identical Mean and SD. B: Average base background of individual animals and their groups (underlined). This metadata can be used to reveal any outlier animals.

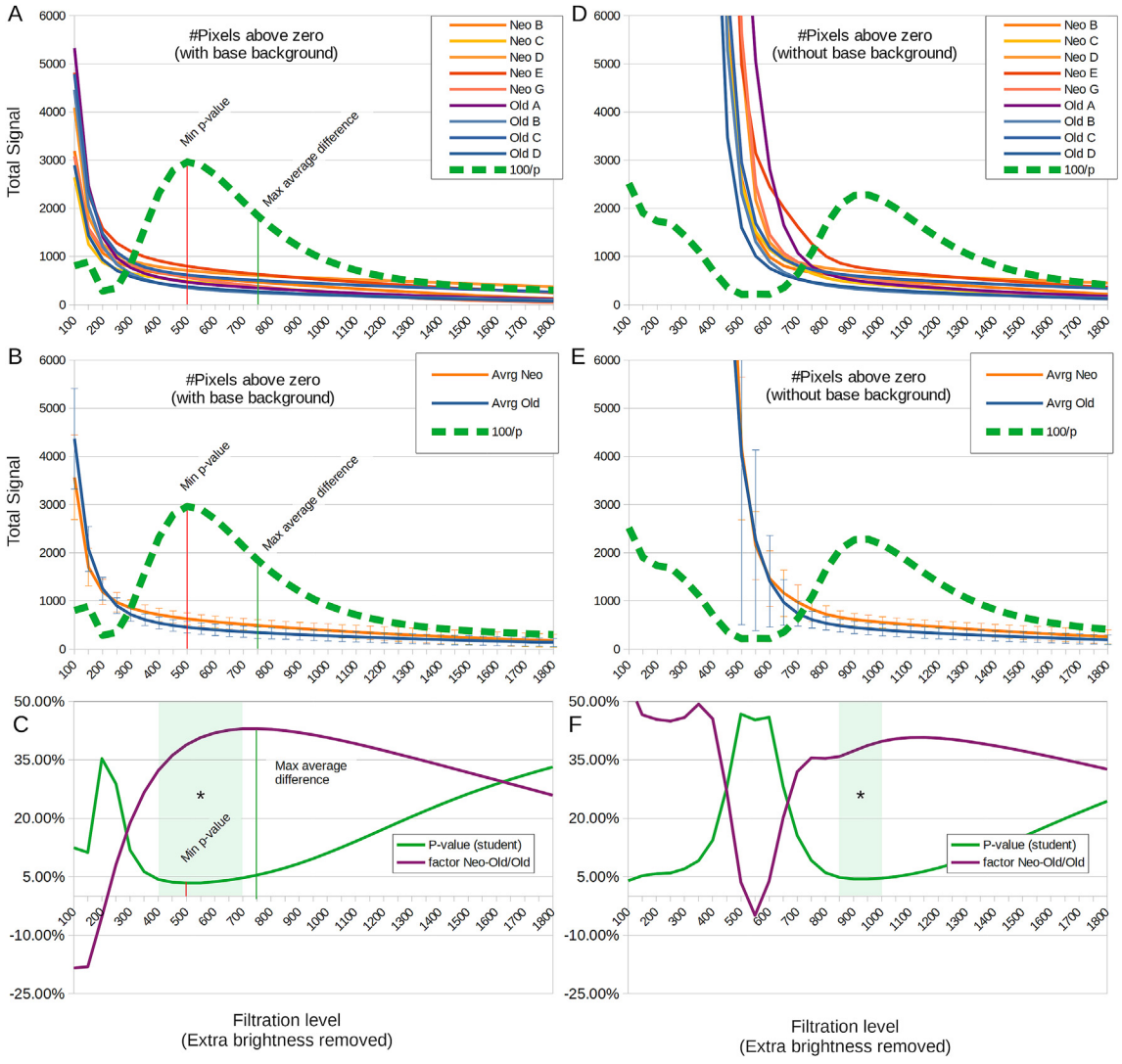

Fig. 6. The process described in Fig. 3 was applied to the entire dataset (9 animals) with and without application of the base background (A, B, C vs D, E, F, respectively). Graphs A, B and C appear similar to graphs D, E and F except shifted a few hundred PBUs to the left because the base background removed several hundred PBUs. For each filtration level, a t-test was run, and the results were converted into the 100/p indicator (green dotted line) for visualization purposes. The indicator was at a maximum at 500 PBU filtration level if applying the base background. At this setting, neonates had a 38.9% stronger signal than older rats. This increase rose to a maximum of 43% if using a 750 BPU filtration level in addition to the base background (graph C). Applying the base background also corrected the two abnormal curves (Old A and Neo E) and reduced the variability among samples, as shown by the error bars (compare filtration levels 100~300 on graph B and filtration levels 500~700 on graph E).

images is far easier on high-contrast pictures, obtaining those often requires dedicated hardware and specific knowledge [10], as well as the foresight to commit beforehand to such high quality. Robust noise filtration systems, on the other hand, mean there is far less need to carefully tailor the imaging protocol, simplifying the operations for the user. Moreover, as the program we present has few prerequisites for running, it can easily be used by other researchers struggling with sorting out signal from noise without necessarily having to form a new dataset of higher quality.

Relying on automation for data extraction and treatment implies relinquishing total certainty. Indeed, we found that our automated background determination step carries a risk of mistakenly labeling authentic hNCAM staining as noise, although it was minimal. It would be more problematic to take “void” squares such as a ventricular area or very high signal-containing squares as background (false positives). However, it was not observed in the data from our quality control subset, as the program includes fail-safes specifically to prevent this from happening (See User Manual in Supplementary Materials).

When comparing the outcome of grafts in different conditions, the survival and proliferation of the grafted material is normally assessed [6,8,12]. Survival and proliferation can be used as a denominator of neurite-extension or other measurements, but this is not always done. This is particularly important in Ref. [2]; who aimed to understand whether more grafted cells can compensate for low survival. In the presented study, the grafted material was obtained through a protocol intended for clinical trials [4] and was previously shown to robustly survive with low proliferation [7]. Accordingly, in the present study, we decided to consider survival and proliferation as identical and null, respectively.

Our system works on the assumption that all genuine hNCAM staining indicates graft-derived material. Thus, the approximately 38–40% increase in the measured signal observed in the neonates means that a younger brain environment is more receptive to the neural grafting of iPSC-derived neurons for the same amount and type of grafted material. This finding is consistent with previous research using ventral mesencephalic tissue [2,3].

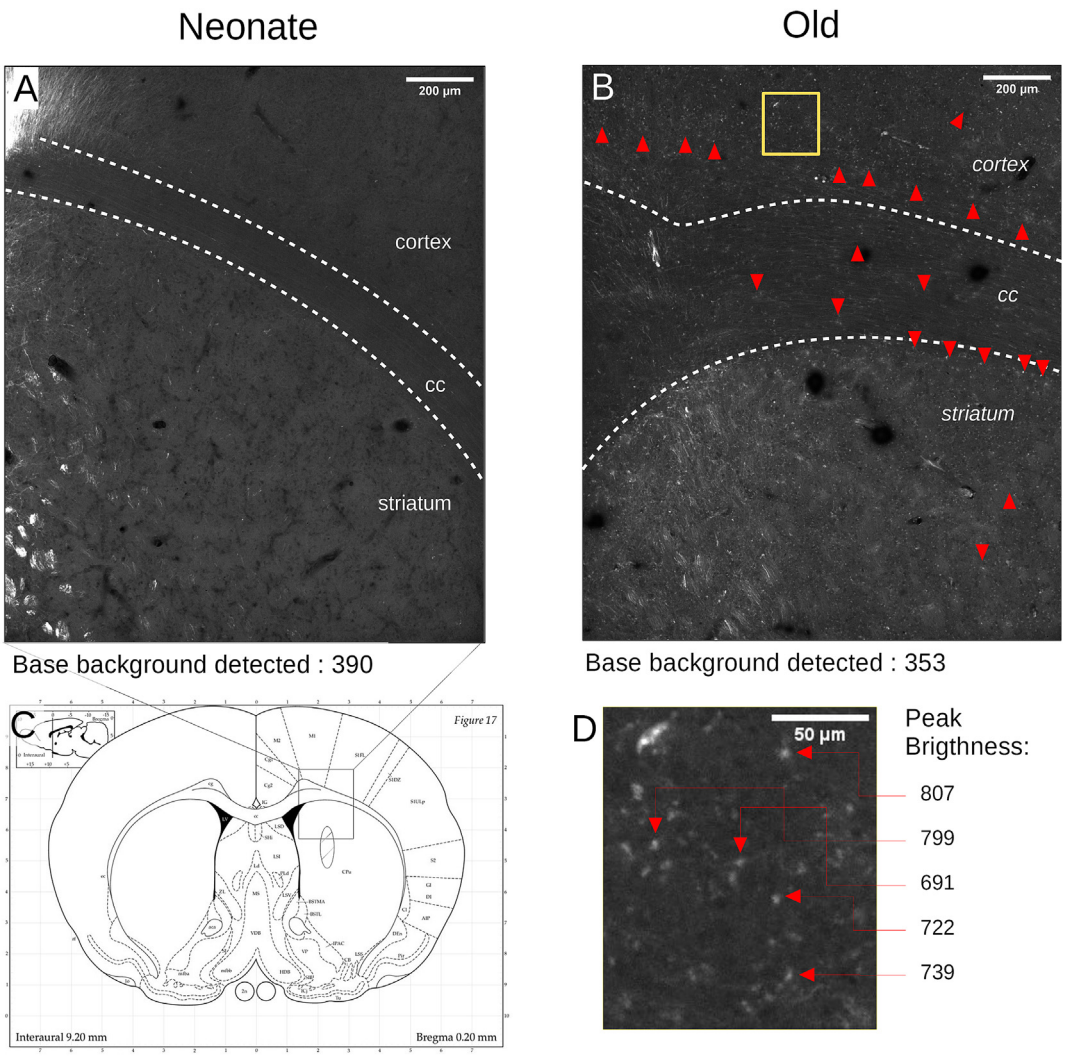

Fig. 7. Numerous specks (red arrowheads) are present in old brains (26-months old at the time of sacrifice) but not in a neonate (2-months old at the time of sacrifice). Both slices (A&B) come from similar locations in the animals (C). The specks are particularly visible in the cortex and corpus callosum but nevertheless are present almost everywhere and pose a serious issue due to their vast number. (D, magnification of the yellow rectangle in the top right image) Removing the specs entirely would require removing up to 800 PBU. Thus, removing 450 PBU in addition to 350 PBU (base background) fits with the filtration levels that show a rise in the indicator in Fig. 6.

Future developments in the field of neural replacement therapies will require both improvements in the material grafted (cell differentiation and possibly conditioning) and the development of drugs aimed at improving the ability of the host brain to accommodate the graft. Our macro is intended to help with the evaluation of these improvements.

Declaration of competing interest

The authors declare that no conflict of interest exists.

Acknowledgments

We thank Dr. Peter Karagiannis for critically reading the manuscript. This study was supported by a grant from the Network Program for Realization of Regenerative Medicine from the Japan Agency for Medical Research and Development (AMED).

Appendix A. Supplementary data

Supplementary data to this article can be found online at https://doi.org/10.1016/j.reth.2022.01.002.

References

[1] Cardoso T, Adler AF, Mattsson B, Hoban DB, Nolbrant S, Wahlestedt JN, et al. Target-specific forebrain projections and appropriate synaptic inputs of hESC-derived dopamine neurons grafted to the midbrain of parkinsonian rats. J Comp Neurol 2018;526:2133–46. https://doi.org/10.1002/cne.24500.
[2] Collier TJ, O'Malley J, Rademacher DJ, Stancati JA, Sisson KA, Sortwell CE, et al. Interrogating the aged striatum: robust survival of grafted dopamine neurons in aging rats produces inferior behavioral recovery and evidence of impaired integration. Neurobiol Dis 2015;77:191–203. https://doi.org/10.1016/j.nbd.2015.03.005.
[3] Collier TJ, Sortwell CE, Daley BF. Diminished viability, growth, and behavioral efficacy of fetal dopamine neuron grafts in aging rats with long-term dopamine depletion: an argument for neurotrophic supplementation. J Neurosci 1999;19:5563–73. https://doi.org/10.1523/jneurosci.19-13-05563.1999.
[4] Doi D, Samata B, Katsukawa M, Kikuchi T, Morizane A, Ono Y, et al. Isolation of human induced pluripotent stem cell-derived dopaminergic progenitors by cell sorting for successful transplantation. Stem Cell Reports 2014;2:337–50. https://doi.org/10.1016/j.stemcr.2014.01.013.
[5] Grealish S, Diguet E, Kirkeby A, Mattsson B, Heuer A, Bramoulle Y, et al. Human ESC-derived dopamine neurons show similar preclinical efficacy and potency to fetal neurons when grafted in a rat model of Parkinson's disease. Cell Stem Cell 2014;15:653–65. https://doi.org/10.1016/j.stem.2014.09.017.
[6] Hargus G, Cooper O, Deleidi M, Levy A, Lee K, Marlow E, et al. Differentiated Parkinson patient-derived induced pluripotent stem cells grow in the adult rodent brain and reduce motor asymmetry in Parkinsonian rats. Proc Natl Acad Sci U S A 2010;107:15921–6. https://doi.org/10.1073/pnas.1010209107.

[7] Kikuchi T, Morizane A, Doi D, Magotani H, Onoe H, Hayashi T, et al. Human iPS cell-derived dopaminergic neurons function in a primate Parkinson's disease model. Nature 2017;548:592–6. https://doi.org/10.1038/nature23664.
[8] Kriks S, Shim JW, Piao J, Ganat YM, Wakeman DR, Xie Z, et al. Dopamine neurons derived from human ES cells efficiently engraft in animal models of Parkinson's disease. Nature 2011;480:547–51. https://doi.org/10.1038/nature10648.
[9] Nakagawa M, Taniguchi Y, Senda S, Takizawa N, Ichisaka T, Asano K, et al. A novel efficient feeder-Free culture system for the derivation of human induced pluripotent stem cells. Sci Rep 2014;4:1–7. https://doi.org/10.1038/srep03594.
[10] Pang Z, barash E, Santamaria-Pang A, Sevinsky C, Li Q, Ginty F. Autofluorescence removal using a customized filter set. Microsc Res Tech 2013;76(10):1007–15. https://doi.org/10.1002/jemt.22261.
[11] Perez-Bouza A, Di Santo S, Seiler S, Meyer M, Andereggen L, Huber A, et al. Simultaneous transplantation of fetal ventral mesencephalic tissue and encapsulated genetically modified cells releasing GDNF in a hemiparkinsonian rat model of Parkinson's disease. Cell Transplant 2017;26:1572–81. https://doi.org/10.1177/0963689717721202.
[12] Rhee YH, Ko JY, Chang MY, Yi SH, Kim D, Kim CH, et al. Protein-based human iPS cells efficiently generate functional dopamine neurons and can treat a rat model of Parkinson disease. J Clin Invest 2011;121:2326–35. https://doi.org/10.1172/JCI45794.
[13] Strömberg I, Bygdeman M, Goldstein M, Seiger Å, Olson L. Human fetal substantia nigra grafted to the dopamine-denervated striatum of immunosuppressed rats: evidence for functional reinnervation. Neurosci Lett 1986;71:271–6. https://doi.org/10.1016/0304-3940(86)90632-4.
[14] Torikoshi S, Morizane A, Shimogawa T, Samata B, Miyamoto S, Takahashi J. Exercise promotes neurite extensions from grafted dopaminergic neurons in the direction of the dorsolateral striatum in Parkinson's disease model rats. J Parkinsons Dis 2020;10:511–21. https://doi.org/10.3233/JPD-191755.